ACS APPLIED MATERIALS & INTERFACES

RESEARCH ARTICLE

www.acsami.org

Nanowires Assembled SnO_2 Nanopolyhedrons with Enhanced Gas Sensing Properties

Di Chen, Jing Xu, Zhong Xie, and Guozhen Shen*

Wuhan National Laboratory for Optoelectronics (WNLO) and College of Optoelectronic Science and Engineering, Huazhong University of Science and Technology (HUST), Wuhan, 430074 (China)

Supporting Information

ABSTRACT: Self-assembly of one-dimensional nanoscale building blocks into functional 2-D or 3-D complex superstructures has stimulated a great deal of interest. We report the synthesis and characterization of nanopolyhedrons assembled from ultrathin SnO_2 nanowires based on the sodium dodecyl sulfate (SDS)-assisted hydrothermal process. As-synthesized SnO_2 nanopolyhedrons have uniform diameters around 300 nm and are self-assembled by numerous ultrathin SnO_2 nanowires with diameters of 5−10 nm. The growth mechanism was also studied by investigating the samples synthesized at different reaction time. Thin films of the assembled SnO_2 nanopolyhedrons were configured as high performance sensors to detect methanol, ethanol, and acetone, which exhibited 1 ppm sensitivity, very fast response and recovery times (several seconds for different gases with concentrations of 1−200 ppm) to all the target gases and highly selective detection to acetone.

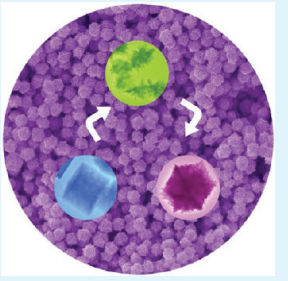

KEYWORDS: nanopolyhedron, SnO_2, nanowires, chemical sensor, hydrothermal, assembly

INTRODUCTION

Assembly of functional nanoscale building blocks into appropriate superstructures is an important prerequisite for electronic and optoelectronic applications.[1−4] Nanotubes, nanowires, nanorods, and nanobelts represent a very unique class of one-dimensional (1-D) nanoscale building blocks.[5−8] Once such 1-D nanoscale building blocks can be ordered and rationally assembled into appropriate two- or three-dimensional architectures, they will offer fundamental scientific opportunities for investigating the influence of size and dimensionality with respect to their collective optical, magnetic, and electronic properties and would provide possibilities to probe brand-new properties and applications resulting from the spatial orientation and arrangement of the nanocrystals.[6−10] Many efforts have been focused on the integration of nanorods/nanowires as building blocks into 2-D or 3-D complex superstructures.[11−15] However, it remains a significant challenge to develop facile, solution-based, and shape-controlled self-assembly routes for the formation of complex architectures from 1-D nanocrystals.

As an important n-type wide-band gap (E_g = 3.6 eV) semiconductor, SnO_2 is one of the most intensively studied materials and has attracted great interest because of its interesting physical properties and important applications in gas sensors, lithium rechargeable batteries, photocatalyst, and dye-sensitized solar cells.[16−23] Although there have been considerable efforts toward the synthesis of 1-D SnO_2 nanomaterials, the shape-specific synthesis and assembly of 1-D SnO_2 nanomaterials into complex functional architectures are still desired for future applications.

In this paper, we report the facile synthesis of faceted SnO_2 polyhedrons self-assembled from small diameters SnO_2 nanowires based on the SDS-assisted hydrothermal process. The formation mechanism was investigated in detail. The as-synthesized SnO_2 nanopolyhedrons were configured as high performance chemical sensors with sensing ability toward 1 ppm level to methanol, ethanol, and acetone. Besides, the sensors have features of very fast response and recovery times (several seconds for different gases with concentrations of 1−200 ppm), and highly selective detection to acetone.

EXPERIMENTAL METHODS

Assembled SnO_2 nanopolyhedrons were synthesized via a simple hydrothermal process. In a typical process, 2 mmol SDS were dissolved in 15 mL distilled water under magnetic stirring to form a transparent solution. Then 0.05 mmol $Zn(Ac)_2$ was added into this solution and the solution was stirred for 2 h. After dissolving 0.5 mmol Na_2SnO_3, the solution was transferred to a Teflon-lined autoclave with 23 mL capacity. The autoclave was put into an oven, which was already heated to 180 °C and kept at that temperature for 20 h. After cooled to room temperature, the obtained white powders were washed with distilled water and absolute ethanol for several times.

The product was characterized using X-ray diffraction (XRD, RINT 2200HF), scanning electron microscopy (SEM, JEOL JSM-6700F) and field-emission transmission electron microscopy (TEM, JEOL, JEM-3000F) equipped with an energy-dispersive X-ray spectrometer (EDS). The UV−vis diffuse reflectance spectrum was measured at room temperature with a UV−vis spectrometer (UV-2500, Shimadzu) and was converted to absorbance spectrum by the Kubelka−Munk method.

RESULTS AND DISCUSSION

X-ray powder diffraction (XRD) was used to characterize the composition and structure of the product and the corresponding

Received: March 16, 2011
Accepted: May 4, 2011
Published: May 04, 2011

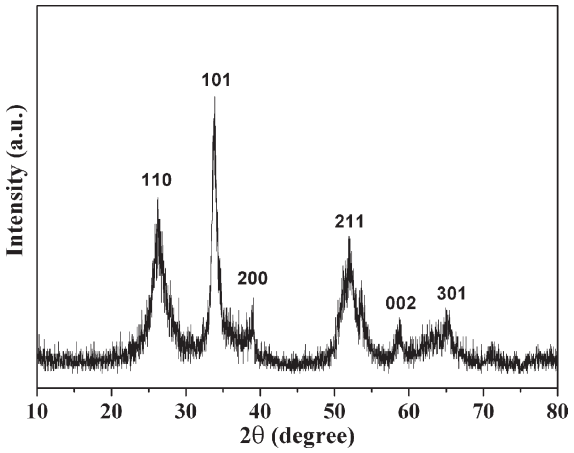

Figure 1. XRD pattern of the as-synthesized SnO_2 product.

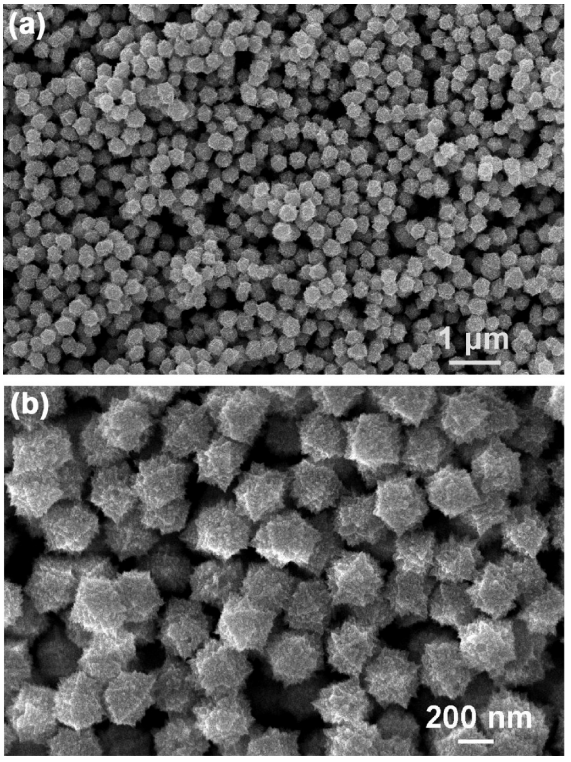

Figure 2. SEM images of as-synthesized product, indicating the formation of SnO_2 nanopolyhedrons assembled by nanowires.

XRD pattern was depicted in Figure 1. All the reflections in the pattern could well be assigned to a pure tetragonal phase of SnO_2 with lattice parameters comparable to the standard values (JCPDS, No. 41−1445). No peaks arising from other crystallized impurities, such as ZnO, $ZnSnO_3$, etc., could be detected, indicating that only SnO_2 grains with good crystallinity and purity were obtained at these conditions. The broadening of the XRD peaks indicates that the products may be with small sizes, which was confirmed as below.

The morphology of the product was studied by using scanning electron microscopy (SEM). Figure 2a shows a low-magnification SEM image of the product. Polyhedron-like nanostructures with uniform sizes were clearly obtained on a large scale. A high-magnification SEM image in Figure 2b shows that typical SnO_2 nanopolyhedron has a diameter of about 300 nm. Contrary to the previously reported nanoparticles-assembled nanopolyhedrons or single-crystalline nanopolyhedrons,[24−27] the present SnO_2 nanopolyhedrons are assembled by numerous ultrathin SnO_2 nanowires.

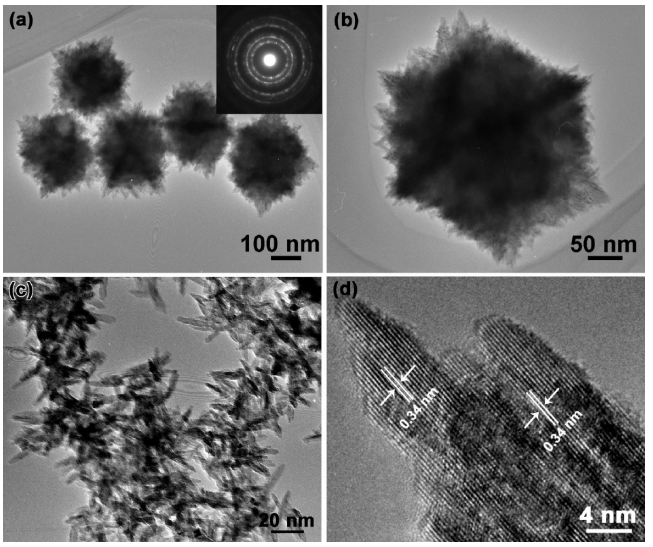

Figure 3. (a) Low-magnification TEM image and SAED pattern of the synthesized SnO_2 nanopolyhedrons. (b) TEM image of individual faceted SnO_2 nanopolyhedron. (c) High-magnification TEM image showing the ultrathin SnO_2 nanowires broken from the nanopolyhedron. (d) Lattice-resolved HRTEM image taken from the tips of several nanowires.

The detailed microstructures of the as-synthesized SnO_2 nanopolyhedrons were investigated by transmission electron microscopy (TEM). Figure 3a shows a low-magnification TEM image, where several SnO_2 nanopolyhedrons can be clearly seen. They have uniform diameters of around 300 nm, in accordance to the SEM results. Selected-area electron diffraction (SAED) pattern depicted in Figure 3a inset reveals the polycrystalline nature of the nanopolyhedrons. The TEM image of a typical SnO_2 nanopolyhedron was shown in Figure 3b. The faceted polyhedron structure can be easily observed from the image. To get clear information about the construction units of the SnO_2 nanopolyhedron, a higher-magnification image taken from the product after ultrasonication was demonstrated in Figure 3c. It confirms that the SnO_2 nanopolyhedron is assembled by numerous ultrathin SnO_2 nanowires with diameter of 5−10 nm with sharp tips, which agrees well with the broaden XRD patterns. Energy dispersive X-ray spectrometer (EDX) was used to investigate the composition of the nanowires, which confirms the formation of pure SnO_2 product (Supporting Information, Figure S1). A high-resolution TEM (HRTEM) image of several SnO_2 nanowires was shown in Figure 3d. The clearly resolved lattice fringes parallel to the length of the nanowires are calculated to be around 0.34 nm, corresponding to the (110) planes of tetragonal rutile SnO_2.

To investigate the detailed formation mechanism of SnO_2 nanopolyhedrons, time-dependent experiments were conducted with all the other conditions keeping constant. Figure 4a is a SEM image of the product after reacting for 5 h. A large quantity of SnO_2 nanocubes with uniform diameters of about 50 nm formed at this stage. When the reaction time was prolonged to 10 h, the

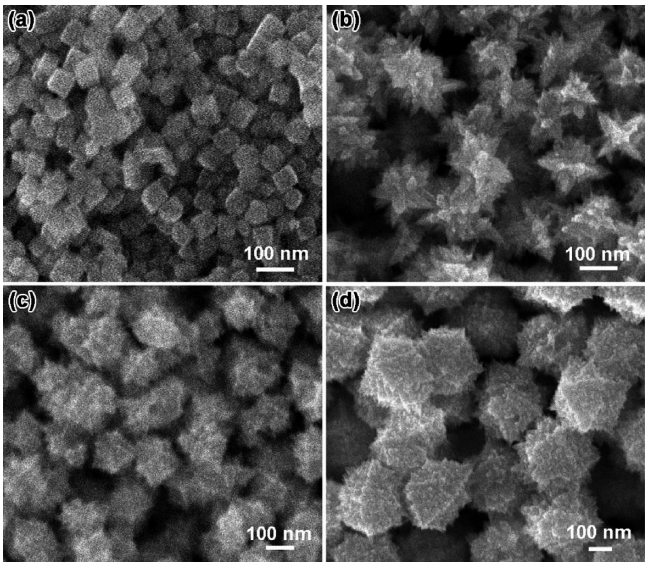

Figure 4. SEM images of the SnO_2 product synthesized at different reaction time: (a) 4, (b) 10, (c) 15, and (d) 24 h.

product was found to be flower-like SnO_2 nanostructures as indicated in Figure 4b. Typical flower-like nanostructures have diameters of ~100 nm. From the size of the nanostructures, it is reasonable to deduce that the SnO_2 nanoflowers are evolved from SnO_2 nanocubes. With the increase of reaction time, the SnO_2 nanoflowers continue growing as indicated in Figure 4c. After growth for 24 h, SnO_2 nanopolyhedrons finally formed as shown in Figure 4d.

On the basis of the time-dependent experiments, we deduced the possible growth mechanism as shown in Scheme 1. In the initial stage, the concentration of both Sn^{4+} and Zn^{2+} are relatively high and the presence of high concentration Zn^{2+} resulted in the formation of SnO_2 nanocubes. To confirm the effect of Zn^{2+}, we did control experiments without the use of $Zn(Ac)_2$ and the product was found to be small SnO_2 nanowires instead of nanocubes (Supporting Information, Figure S2). As the reaction went on, the concentration of Zn^{2+} decreased dramatically and SnO_2 nanoflowers consist of wire-like units began to evolve from the newly formed SnO_2 nanocubes under hydrothermal condition. Continuous growth of SnO_2 nanowires resulted into the final SnO_2 nanopolyhedrons. During the reaction, the surfactant SDS plays an important role for the growth. To confirm the speculation, we did control experiments by substituting SDS with other surfactants, for example, PVA, CTAB, PVP, etc., and kept other conditions constant. Without SDS, no nanopolyhedrons were obtained and the products were either SnO_2 nanoparticles, nanowires, or hierarchical nanowires.

The UV−vis absorption spectrum of the SnO_2 nanopolyhedrons was measured and the result was depicted in Figure 5b. For a comparison, the absorption spectrum of bulk SnO_2 was also measured and the data were shown in Figure 5a. From the spectra, it can be seen that strong absorption of the SnO_2 samples appeared in the ultraviolet region near the visible-light region. The energy gap of the samples, estimated from the plots of $(\alpha h\nu)^2$ vs $h\nu$, was calculated to be around 4.0 eV, which is a bit blue-shifted compared with the bulk material. The blue shift is obviously due to the ultrafine size of the SnO_2 nanopolyhedrons.

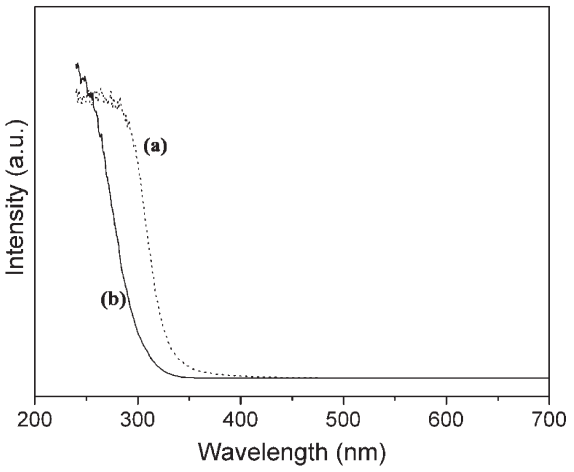

Figure 5. UV−vis diffuse reflectance spectra of (a) bulk SnO_2 powders and (b) the synthesized SnO_2 nanopolyhedrons.

SnO_2 nanostructures have been widely studied as chemical sensors for various toxic or pollution gases/chemicals, such as O_2, NO_2, CO, H_2, methanol, ethanol, acetone, etc.[28−33] The sensing performance is greatly influenced by the size, structure and morphology of the SnO_2 nanostructures since the sensing behavior is a prominently surface-dependent phenomenon. We also investigated the chemical sensing properties of the SnO_2 nanopolyhedrons here.

To fabricate a SnO_2 nanopolyhedrons based gas sensor, the as-grown SnO_2 nanopolyhedrons were mixed and ground with an adhesive in an agate mortar to form a gas sensing paste. The paste was coated onto an alumina tube on which a pair of Au electrodes was previously printed. After dried in air for several minutes, the alumina with coated nanopolyhedrons was annealed at 400 °C for 2 h to improve the mechanical strength. After being welded onto the pedestal, the gas sensors were aged for 72 h by applying 5 V on the heating wire. To research the influence of operating temperature and to get an optimum operating temperature, we tested the responses of SnO_2 gas sensors to 20 ppm acetone as a function of operating temperature and the result was shown in Figure 6a. From the curve, it was seen that the sensing response first increased with temperature, up to 370 °C, and then decreased. The maximum sensitivity reaches 17.5 at 370 °C. Thus the optimized 370 °C was chosen for further gas sensing tests of the SnO_2 nanopolyhedron. Figure 6b shows the representative dynamic gas response of the SnO_2 gas sensor to acetone with concentrations ranging from 1 ppm to 200 ppm when the sensor worked at 370 °C. Seven cycles were successively recorded, corresponding to seven different acetone concentrations of 1, 10, 20, 40, 100, 150, and 200 ppm, respectively. From the curves, it can be seen that the conductance of the sensor undergoes a drastic rise upon the injection of acetone and drops to its initial state after the sensor was exposed to air. The sensitivity of the sensor to 1 ppm acetone is around 4 and to 200 ppm acetone is around 48, respectively. It indicates that the sensing detection limit is rather good for the SnO_2 nanopolyhedrons. The gas sensing response and recovery times are important parameters to evaluate the performance of a gas sensor. Figure 6c and 6d are the sensing curves of the SnO_2 nanopolyhedrons sensor to acetone with concentrations of 1 ppm and 200 ppm, respectively. Measured from the curves, it was found that the sensing response and recovery times were 7s and 2.6s for 1

Scheme 1. Schematic Illustration of the Possible Growth Process

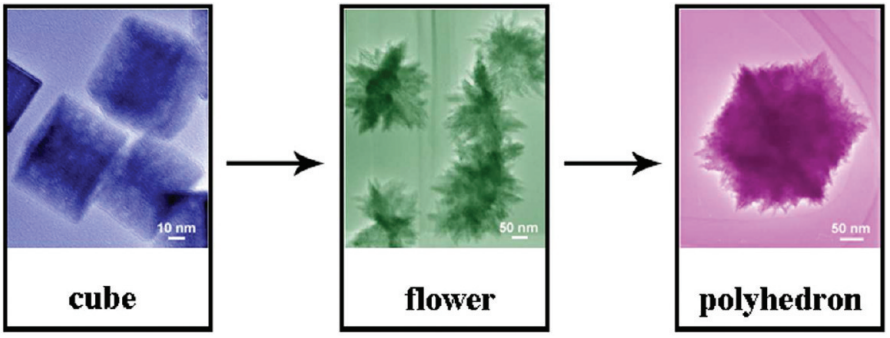

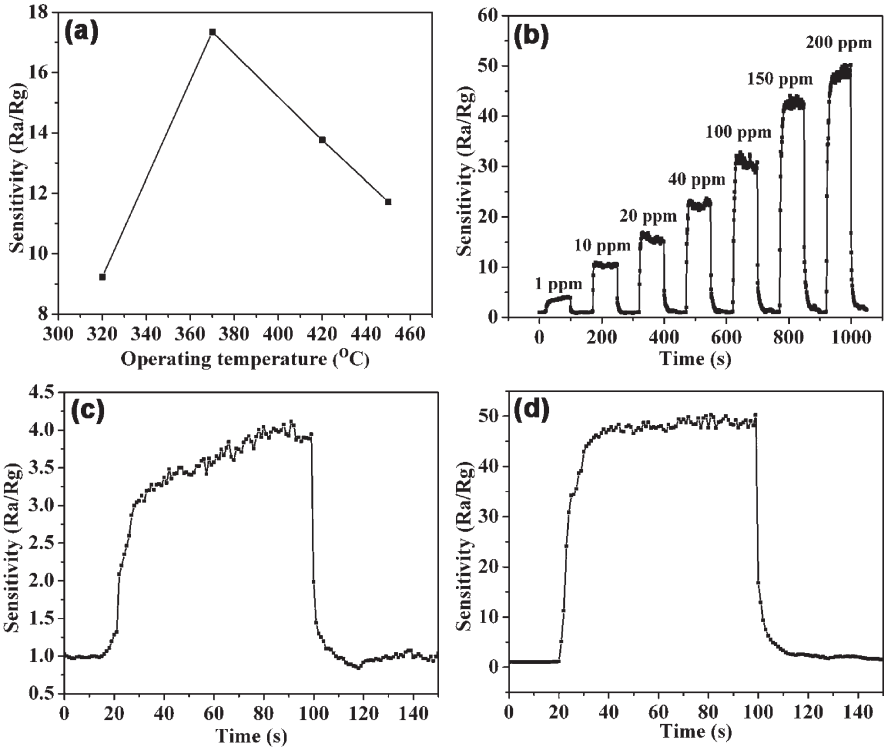

Figure 6. (a) Sensor sensitivity vs. operating temperature of the synthesized SnO_2 polyhedrons. (b) Dynamic response-recovery curves of the gas sensors built on the synthesized SnO_2 polyhedrons to acetone with varied concentrations. (c,d) Dynamic response-recovery curves of the gas sensors to 1 ppm and 200 ppm acetone, respectively.

ppm acetone, 9.7s and 5.8s for 200 ppm acetone, respectively, indicating fast sensing ability of the SnO_2 nanopolyhedrons sensor.

The sensing characteristics of the SnO_2 nanopolyhedrons sensor to methanol and ethanol were also studied. Figure 7 shows the dynamic gas response of the SnO_2 gas sensor to methanol and ethanol with different concentrations, respectively. Seven cycles were recorded, according to the gas concentration of 1, 10, 20, 40, 100, 150, and 200 ppm, respectively. Similar to the sensing characteristics of the sensor to acetone, the conductance of the sensor undergoes a drastic rise upon the injection of gases and drops to its initial state after the sensor was exposed to air. The lowest detection limit of the sensor was down to 1 ppm methanol with a sensitivity of 1.8 and 1 ppm ethanol with a sensitivity of 2.6, respectively.

We also investigated the gas sensing properties of different SnO_2 materials, including the current nanowires assembled SnO_2 nanopolyhedrons, SnO_2 nanowires, and commercial powders to depict the enhanced gas sensing performance of the nanowire assembled SnO_2 nanopolyhedrons. As examples, Figure 8 shows the relationship between sensor response and gas concentrations of acetone and ethanol, respectively. From the curves, it is obviously that sensors based on nanowires assembled SnO_2 nanopolyhedrons exhibit much higher response to both gases than SnO_2 nanowires and bulk material. For example, the response values of the nanowire assembled SnO_2 nanopolyhedrons, SnO_2 nanowires, and commercial powders are 50.2, 25.6, and 18.8, respectively, when the acetone concentration is fixed at 100 ppm. Similar trend was also observed for the detection of ethanol.

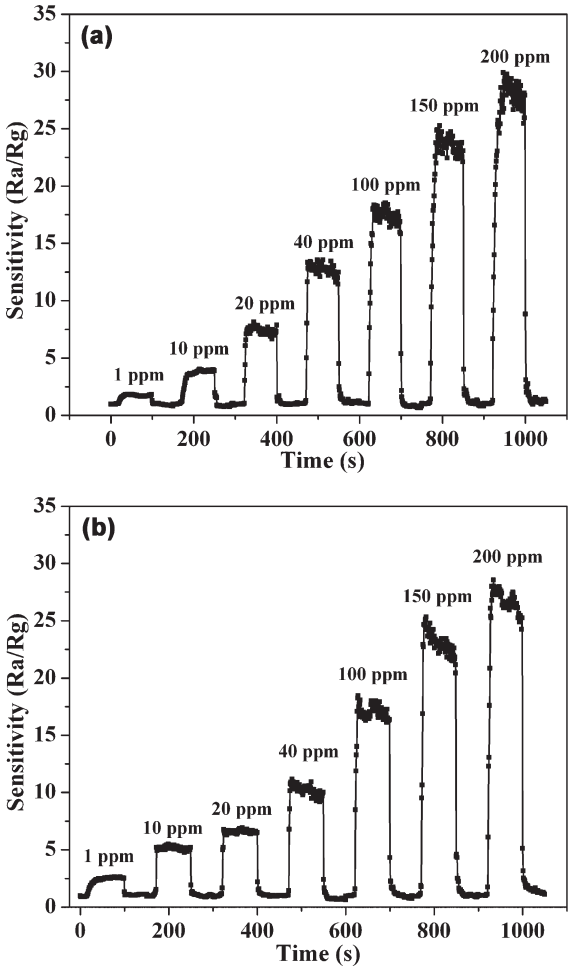

Figure 7. Dynamic response-recovery curves of the gas sensors built on the synthesized SnO_2 polyhedrons to (a) methanol, and (b) ethanol, with varied concentrations ranging from 1 ppm to 200 ppm.

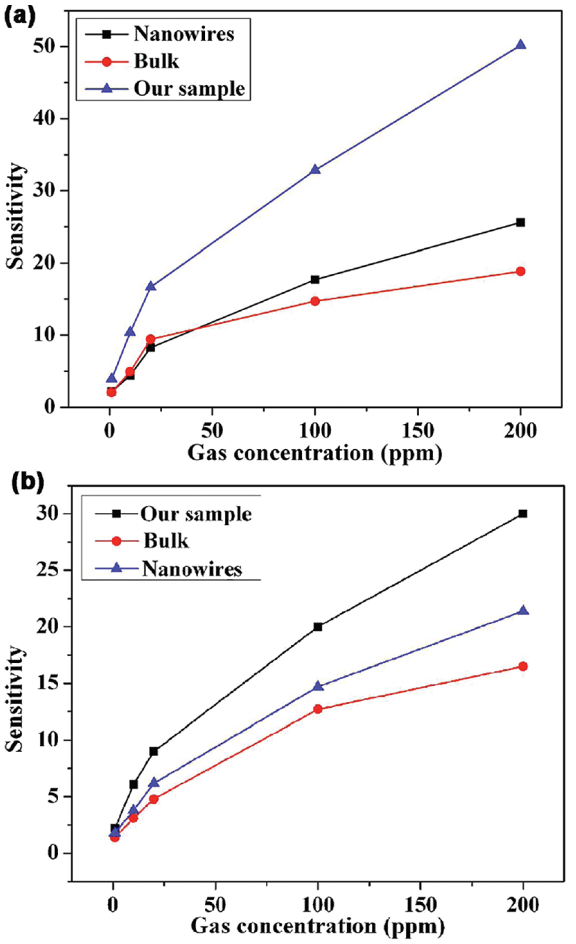

Figure 8. Relationship between sensor response and gas concentrations of acetone and ethanol, respectively, built on the nanowire assembled SnO_2 nanopolyhedrons, nanowires, and commercial powders.

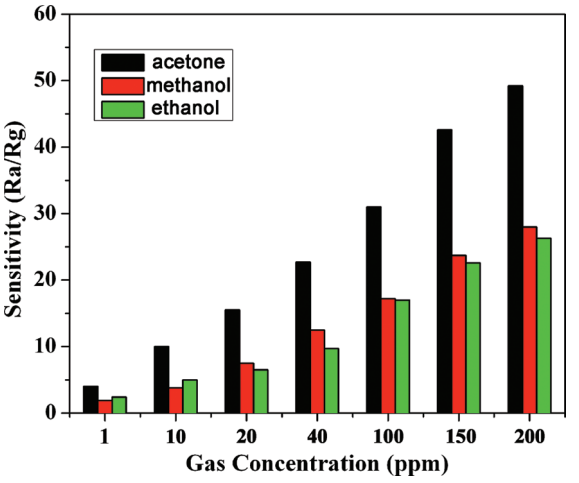

Figure 9. Response values of the gas sensors built on the synthesized SnO_2 polyhedrons to different gases of 200 ppm. (The error limits is around ±0.1.)

It is well-known that the gas sensing mechanism of metal oxide semiconductor is an adsorption-oxidation-desorption process leading to the change of the conductance of the sensor. To explain the excellent gas sensing performance of the as-synthesized SnO_2 nanopolyhedrons, the following factor should be considered. According to the model of the grain size effect in n-type semiconducting metal oxide gas sensors,[34] when $D \leq 2L$ (L is the thickness of the depletion layer), the gas sensors perform better. As shown in Figure 3c, the SnO_2 nanowires within nanopolyhedrons have diameters of around 3−5 nm, which is smaller than $2L$ of SnO_2 (L = 3 nm, thickness of the depletion layer) and contributes most to the gas sensing response.

To get clear information about the sensing selectivity of the SnO_2 nanopolyhedrons sensor, we compared the sensing ability among methanol, ethanol, and acetone and the results are demonstrated in Figure 9. From the data shown in Figure 9, we can see that the sensitivity of the SnO_2 nanopolyhedrons sensor showed superior sensitivity to acetone than methanol and ethanol with concentrations ranging from 1 ppm to 200 ppm, indicating very good selectivity to acetone among three chemicals. As we know, SnO_2 usually shows better sensitivity to ethanol than acetone. However, for the nanowires assembled SnO_2 nanopolyhedrons here, they showed better sensitivity to acetone than ethanol. Based on our experiments, we believed that under the current experimental conditions, SnO_2 products were doped with trace Zn^{2+}, though we did not observed the signals of Zn element by XRD and EDX. According to previous studies, the

use of proper dopants could greatly change the selectivity of SnO_2 nanostructures.[34−37] Thus, we deduced that the introduce of $Zn(Ac)_2$ into the reaction system is the main reason for the selective detection of acetone. The speculation was confirmed from the results shown in Figure 8, where no obvious selectivity to acetone was observed for pure SnO_2 nanowires synthesized in the absence of $Zn(Ac)_2$.

In conclusion, we successfully synthesized SnO_2 nanopolyhedrons assembled from ultrathin SnO_2 nanowires based on the sodium dodecyl sulfate (SDS)-assisted hydrothermal process. The growth process was studied and it was found that SDS plays an important role for the assembly process. The as-obtained SnO_2 nanopolyhedrons exhibited 1 ppm sensitivity to all the chemicals, very fast response and recovery times (several seconds for different gases with concentrations of 1−200 ppm), and highly selective detection to acetone. Our results suggest that the SnO_2 nanopolyhedrons are promising candidates for high performance chemical sensors in terms of detection limit, sensitivity, and selectivity.

■ ASSOCIATED CONTENT

Supporting Information. EDX spectrum of the as-obtained SnO_2 nanowires, SEM images of the SnO_2 products synthesized in the absence of $Zn(Ac)_2$. This information is available free of charge via the Internet at http://pubs.acs.org.

■ AUTHOR INFORMATION

Corresponding Author
*E-mail: gzshen@mail.hust.edu.cn.

■ ACKNOWLEDGMENT

This work was supported by National Natural Science Foundation of China (51002059, 21001046), the 973 Program of China (2011CBA00700), the Natural Science Foundation of Hubei Province (2009CDB326), the Research Fund for the Doctoral Program of Higher Education (20090142120059, 20100142120053) and the High-level Talent Recruitment Foundation of Huazhong University of Science and Technology and the Director Fund of WNLO. Special thanks to the Analytical and Testing Center of HUST for using their facilities.

■ REFERENCES

(1) Shi, H. T.; Qi, L. M.; Ma, J. M.; Cheng, H. M. *J. Am. Chem. Soc.* **2003**, *125*, 3450–3451.
(2) Shen, G. Z.; Chen, D. *J. Am. Chem. Soc.* **2006**, *128*, 11762–11763.
(3) Chen, D.; Ye, J. H. *Adv. Funct. Mater.* **2008**, *18*, 1922–1928.
(4) Yu, S. H.; Colfen, H.; Tauer, K.; Antonietti, M. *Nat. Mater.* **2005**, *5*, 51–55.
(5) Kong, X. Y.; Ding, Y.; Yang, R. S.; Wang, Z. L. *Science* **2004**, *303*, 1348–1351.
(6) Manna, L.; Scher, E. C.; Alivisatos, A. P. *J. Am. Chem. Soc.* **2000**, *122*, 12700–12706.
(7) Shen, G. Z.; Chen, D. *J. Mater. Chem.* **2011**, *20*, 10888–10893.
(8) Li, M.; Schnablegger, H.; Mann, S. *Nature* **1999**, *402*, 393–395.
(9) Amelinekx, S.; Zhang, X. B.; Bernacrts, D.; Zhang, X. F.; Ivanov, V.; Nagy, J. B. *Science* **1994**, *265*, 635–639.
(10) Gudiksen, M. S.; Lauhon, L. J.; Wang, L.; Smith, D. C.; Lieber, C. M. *Nature* **2002**, *415*, 617–620.
(11) Shen, G. Z.; Xu, J.; Wang, X. F.; Huang, H. T.; Chen, D. *Adv. Mater.* **2011**, *23*, 771–775.
(12) Lu, W.; Gao, P.; Jian, W. B.; Wang, Z. L.; Fang, J. *J. Am. Chem. Soc.* **2004**, *126*, 14816–14821.
(13) Algra, R. E.; Verheijen, M. A.; Borgstrom, M. T.; Feiner, L. F.; Immink, G.; van Enckevort, W. J. P.; Vlieg, E.; Bakkers, E. P. A. M. *Nature* **2008**, *456*, 369–372.
(14) Kong, X. Y.; Ding, Y.; Yang, R.; Wang, Z. L. *Scinece* **2004**, *303*, 1348–1351.
(15) Shen, G. Z.; Bando, Y.; Hu, J.; Golberg, D. *Appl. Phys. Lett.* **2007**, *90*, 123101.
(16) Gubbala, S.; Chakrapani, V.; Kumar, V.; Sunkara, M. K. *Adv. Funct. Mater.* **2008**, *18*, 2411–2418.
(17) Liu, Z.; Zhang, D.; Han, S.; Li, C.; Tang, T.; Jin, W.; Liu, X.; Lei, B.; Zhou, C. *Adv. Mater.* **2003**, *15*, 1754.
(18) Lu, J. G.; Chang, P.; Fan, Z. *Mater. Sci. Eng., R* **2006**, *52*, 49–91.
(19) Cheng, Y.; Xiong, P.; Yun, C. S.; Strouse, G. F.; Zheng, J. P.; Yang, R. S.; Wang, Z. L. *Nano Lett.* **2008**, *8*, 4179–4184.
(20) Wang, Y. L.; Jiang, C. C.; Xia, Y. N. *J. Am. Chem. Soc.* **2003**, *125*, 16176–16177.
(21) Kuang, Q.; Lao, C.; Wang, Z. L.; Xie, Z.; Zheng, L. *J. Am. Chem. Soc.* **2007**, *129*, 6070–6071.
(22) Mathur, S.; Barth, S. *Small* **2007**, *3*, 2070–2075.
(23) Shen, G. Z.; Chen, P. C.; Zhou, C. W. *J. Mater. Chem.* **2009**, *19*, 828–839.
(24) Sun, Y.; Xia, Y. *Science* **2002**, *298*, 2176–2179.
(25) Gao, P. X.; Wang, Z. L. *J. Am. Chem. Soc.* **2003**, *125*, 11299–11305.
(26) Cao, H. L.; Qian, X. F.; Wang, C.; Ma, X. D.; Yin, J.; Zhu, Z. K. *J. Am. Chem. Soc.* **2005**, *127*, 16024–1625.
(27) Jiang, H.; Geng, B. Y.; Kuai, L.; Wang, S. Z. *Chem. Commun.* **2011**, *47*, 2447–2449.
(28) Sysoev, V. V.; Schneider, T.; Goschnick, J.; Kiselev, I.; Habicht, W.; Hahn, H.; Strelcov, E.; Kolmakov, A. *Sens. Actuators B* **2009**, *139*, 699–703.
(29) Sysoev, V. V.; Goschnick, J.; Schneider, T.; Strelcov, E.; Kolmakov, A. *Nano Lett.* **2007**, *7*, 3182–3188.
(30) Kolmakov, A.; Klenov, D. O.; Lilach, Y.; Stemmer, S.; Moskovits, M. *Nano Lett.* **2005**, *5*, 667–673.
(31) Kolmakov, A.; Zhang, Y.; Cheng, G.; Moskovits, M. *Adv. Mater.* **2003**, *15*, 997–1000.
(32) Wan, Q.; Huang, J.; Xie, Z.; Wang, T. H.; Dattoli, E. N.; Lu, W. *Appl. Phys. Lett.* **2008**, *92*, 102101.
(33) Wang, Q.; Wang, T. H. *Chem. Commun.* **2005**, *30*, 3841–3843.
(34) Rothschild, A.; Komem, Y. *J. Appl. Phys.* **2004**, *95*, 6374–6380.
(35) Ding, X. H.; Zeng, D. W.; Xie, C. S. *Sens. Actuators B* **2010**, *149*, 336–344.
(36) Zima, A.; Kock, A.; Maier, T. *Microelectron. Eng.* **2010**, *87*, 1467–1470.
(37) Jiang, Z. W.; Guo, Z.; Sun, B.; Jia, Y.; Li, M. Q.; Liu, J. H. *Sens. Actuacotrs B* **2010**, *145*, 667–673.